Chapter 6

Fabrication of Curved Structures with Electron Beam and Surface Structure Characterization

Abstract

In this Chapter, we propose a fabrication technology for preparing curved structures using an electron beam writing strategy. Oxygen plasma treatment increases the surface roughness of SU-8 polymer, while minimizing the outgassing problem and stabilizing the SU-8 film. Fourier transform infrared spectra of epoxy bond near 915 cm^{-1} decreased upon increasing the dosage of the electron beam or the treatment time of the oxygen plasma. Convex, concave, and spiral structures were formed successfully using a gradient dosing strategy. The interface between two shot sections was smoothed by the electron scattering effect. The curved profile was fabricated at various curvatures, and characterized using scanning electron microscopy and a profiler. In addition, a spiral structure was fabricated that possesses the advantageous feature of having a small chip area. We discuss a method of characterizing the spiral structure.

6.1 INTRODUCTION

Integrating micromachine structures and microelectronics into biological systems has become the subject of much recent interest in the biological and medical research communities. Because small sample volumes are employed, fabricated microfluidic devices have the potential for application for highly efficient, multidimensional separations. Rapid progress in micromechanic, microfluidic, and micro-optic device production has propelled the development of methods for binary high aspect ratio structure formation in relatively thick resist layers by deep x ray and photolithography.[1–3] However, further progress in these areas is connected to the development of fabrication technology, which will be able to produce gray scale structures with a continuous surface relief.

Several lithographic techniques for nonplanar production have been developed such as stereolithography and focused ion-beam deposition. Stereolithography can be used to fabricate three-dimensional (3D) and high aspect ratio microstructures with low manufacturing cost and short fabrication time. Stereolithography also customizes the packages for microfluidics and microsensors to eliminate the dead volume of the reaction chamber.[4] Fabrication of microelectromechanical systems (MEMS) packages on a wafer level scale can decrease the manufacturing and assembly times. Stereolithography has been applied to chemical sensors, interdigital electrodes, and an atomic force microscope (AFM) Cantilever fluid cell package.[5] However, the stereolithography uses an optical source to illuminate the resist and the pattern resolution is restricted. Focused ions beam micromachining and focused ion beam deposition enable spatially selective, maskless, patterning, and processing of materials at extremely high levels of resolution.[6–8] State-of-the-art focused ion beam columns based on high brightness liquid metal ion source (LMIS) technology are capable of forming probes with dimensions of 10 nm with a lower limit on spot size

set by the inherent energy spread of the LMIS and the chromatic aberration of ion optical systems.[9] However, the printing speed of the ion beam-based techniques is very slow and time consuming. The development of techniques for preparing curved microfluidic channels, such as concave, convex, and spiral structures, will benefit future biodevice applications of which the fluids in the microchannels are delivered by electrokinetic flow.[10] Curved microfluidic structures have the advantage of having smaller chip surface areas than do planar designs having the same flow distance.

The techniques developed for curved structure can be divided into two main groups such as those based on gray scale exposure [4–6] and others based on resist thermal flow during high-temperature baking.[11] Electron beam-based technologies have been predicted to demonstrate the potential capability for future small volume production.[12] The shaped electron-beam writing technology, so-called maskless processing, is a promising means for controlling and patterning small features.[11] The shaped electron beam exhibits higher throughput than the ion beam technique due to imposing several thousand pixels per shot. The thermal flow technique [11] needs to apply the flow temperature on the polymer, but the desired curvature of the sidewall is not easily controlled and achieved. Therefore, the development of writing strategy for the curved structure of interest is inevitable.

The negative chemically amplified photoresist SU-8, a commercial epoxy-based material, was developed for high aspect ratio structure for MEMS. This resist has very good mechanics, and excellent sensitivity, thermal stability, etching resistance, optical properties, and a high sensitivity to 365 nm ultraviolet (UV) radiation, x rays, and electron beam.[13–16] Conventionally, most SU-8 based materials prepared from thick or ultrathick films by using conventional UV or x-ray exposure were used to

fabricate micromachine systems with planar and high-aspect-ratio patterns and were focused mainly on their mechanical applications.[14,15] Kudryashov *et al.* combined electron beam and optical exposures for achieving a 3D structure. This structure demonstrated the step pattern with vertical and horizontal profile.[13,16] In a review Chapter for the fabrication of polymer microfluidic devices,[17] various polymers were reported to become the channel materials. However, the patterning technology for the fabrication of curved structures with shaped electron beam proximity has not been reported.

In this work, the required contrast, the etching resistance, and the thermal stability of SU-8 resist were investigated. Various electron-beam-based writing strategies for the preparation of concave, convex, and spiral structures were proposed and then characterization by scanning electron microscopy (SEM) and surface profiler. In addition, we evaluated the surface properties and morphologies of SU-8 resists after treatment with oxygen plasma. Finally, we propose strategies for printing a spiral channel by electron-beam writing.

6.2 EXPRIMENT

The SU-8 resist, which was obtained from the Microchem Company (Massachusetts), was used to fabricate curved structures with the aid of an electron beam. The ingredients of the resist provided from the vendor were 50%–70% epoxy resin, 25%–50% γ-butyrolactone, and 1%–5% propylene carbonate and triarylsulfonium hexafluoroantimonate salts. Electron-beam exposure was carried out using a Leica Weprint Model-200 stepper (Jena, Germany). The shaped electron-beam energy was 40 kV with a beam size of 20 nm and a beam current of 40 A/cm^2. The developer for the SU-8 resist was a 98%–100% 1-methoxy-2-propyl

acetate solution.

The SU-8 resists were spun onto 6 in. silicon wafers, with resist thicknesses of ~59, 28, and 17 μm at spin rates of 3000, 4500, and 6000 rpm for 0.5 min, followed by a softbaking process for 10 min at 65 °C and 2 min at 90 °C. Fourier transform infrared (FTIR) spectroscopy (Bio-Rad, Model FTS-40, Massachusetts) was used to analyze variations in the resist structure during shaped electron-beam exposure. The film outgassing was determined using a Hitachi thermal desorption system (TDS) model UG-21 (Tokyo, Japan) in conjunction with an atmospheric-pressure-ionization mass spectrometer (APIMS) model UG-400P. The desorption temperature was programmed from room temperature to 300 °C at a ramp rate of 3 °C/min. Oxygen plasma treatment was carried out in a plasma-enhanced chemical vapor deposition chamber (STS, U.K.). The operating frequency was 380 kHz and the power was 250 W. The surface roughness and microscale profile were measured using an AFM (Digital Instruments, DI-5000, USA). The morphology was evaluated with a cross-sectional SEM (Hitachi S-4000). The profile on the surface was evaluated with a Profiler P-10 (TENCOR, U.S.A.). Silicon oxide and poly-Si films were etched using a reactive-ion etcher (RIE) (Tokyo Electron Limited, Model TE5000, Japan) and an electron cyclotron resonance (ECR) etcher (Anelva ECR-6001, Japan), and the operating conditions of etchers were listed in Tables I and II, respectively.

6.3 RESULTS AND DISCUSSIONS

6.3.1 Sensitivity Curve and FTIR Characterization

In general, the fabrication of planar structures requires high-contrast conditions for patterning and ensuring that vertical sidewalls are formed.[18,19] In contrast, fabrication of nonplanar structures requires conditions of low contrast. Figure 6-1

displays the sensitivity curves of SU-8 films at various thicknesses. The contrast and writing time both decrease with decreasing film thickness. This observation suggests that the most-suitable condition for fabricating the nonplanar structures, such as concave, convex, and spiral structures, is the use of a 6000 rpm spinning rate.

Figure 6-2 illustrates FTIR spectra of SU-8 films obtained after various shaped electron-beam doses. The characteristic absorption near 915 cm^{-1}, which we assign to the vibration of epoxy bond, is a suitable probe in the FTIR spectra shown in Figure 6-2 (a).[20] This absorption decreases upon increasing the dosage of the electron beam. The phenomenon suggests that ring opening of epoxy bond occurs after irradiation with the electron beam. In contrast, absorptions appear for the vibrations of C–O–C and O–H units after electron-beam exposure, as is illustrated by Figures 6-2(b) and 2(c). These absorption peaks are also ascribed to ring opening of epoxy units.[21] In the SU-8 film, irradiation with the electron beam first detaches detaches the hardeners, which produces hydroxyl-containing components. These hydroxyl groups induce the ring opening reaction by attacking the epoxy units, which causes a chain reaction that leads to hydroxyl groups being formed. Thus, the intensity of the characteristic absorption near 3450 cm^{-1} increases [Figure 6-2(c)] upon further exposure to the electron beam. The detailed reaction mechanism is illustrated in Figure 6-2(d).

6.3.2 Thermal Stability and Surface Microstructure after Oxygen Plasma Treatment

The thermal stability of SU-8 films, with and without 60 s oxygen plasma treatment, was analyzed using TDS–APIMS. The outgassing mass spectra of SU-8 films from 70 to 300 °C are demonstrated in Figure 6-3(a). Masses of 18, 30, and 44

Daltons represent water (H_2O), ethane (C_2H_6), and propane (C_3H_8), respectively. The film that was not treated with plasma has a broad and characteristic water peak at 200 °C, which represents the water that exists in SU-8 films. This water peak is not observed, however, after plasma treatment has occurred. Similarly, ethane and propane species are also removed by plasma treatment. This finding clearly suggests that treatment with oxygen plasma can stabilize the film, and that the film is thermally stable at up to 300 °C. Figures 6-3 (b) and 6-3 (c) display macroscopic surface SEM images of the SU-8 film that has been treated with oxygen plasma for 60 s. The film's surface has no regular structure, and the surface is uneven. Small holes and cracks are present as well as a slight orientation across the image. The cross-sectional SEM micrograph reveals some deep and large ripples on the surface of the SU-8 film. Figure 6-4 displays AFM micrographs obtained after plasma treatment at various times. The surface profile changes with the plasma treatment time. Nano-nodular structures grow from the film surface during the plasma treatment. After plasma treatment for 60 s, the diameters of the nodules are ~30–40 nm with heights of also 30–40 nm. The formation of nodular structures is partially dependent on cross-linking of the polymer under oxygen plasma in the chamber with temperature of 300 °C. Electronegative atoms and ions of oxygen plasma initiate the ring-open reaction of epoxy resin by attacking the SU-8 resist, then the thermal effect drives the propagation of crosslink reaction to form the nodules structure. The evidence of polymerization of SU-8 resist with oxygen plasma treatment time is shown in Figure 6-5(a). The characteristic absorption near 915 cm^{-1}, the epoxy bond probe in the FTIR spectra, decreases with reaction time, suggesting that the degree of polymerization increases with plasma time. We estimate their roughness, as displayed in Figure 6-5(b), from a 5 X 5 μm image. The surface roughness is due to the increased formation of surface nodules with increasing plasma treatment time.

6.3.3 Fabrication of Convex and Concave Structures

Figure 6-6(a) demonstrates the application of this dosage strategy toward fabricating a convex structure. The electron-beam dosage on unit distance was increased equally at 2 μC/cm^2. The various curvatures are obtained by only changing the length of the unit distance. The steep step height between adjacent dosing sections is not observed in Figure 6-6. This observation of curved structure is explained by the scattering effect of the electron beam from neighboring sections. Figure 6-6 also indicates that the curvature increases upon decreasing the length of the unit distance. This phenomenon is dependent on the dose density on a fixed area. The higher dose density induces more cross-linkage reactions of the SU-8 polymer. Table III summarizes the mathematical convex relationship between the film thickness and the scanning distance from P-10 measurements. These convex equations can be used to predict the profiles obtained by various dosing strategies. Figures 6(b)–6(e) clearly depict that the dosing strategy can print various convex structures. These SEM micrographs demonstrate the same behavior observed in the P-10 profiles in Figure 6-6(a). Therefore, this core technology developed for fabricating nonplanar structures will be beneficial for the future fabrication of devices.

Figure 6-7(a) depicts a patterning strategy for the fabrication of concave structures. The electron-beam dosage on unit distance is increased. The various curves are obtained by only changing the length of the unit distance. Figure 6-7 also indicates that the curvature increases with decreasing length of the unit distance. This phenomenon is dependent on the dose density on a fixed area. The higher dose density induces more cross-linking reactions of the SU-8 polymer. Table III summarizes the mathematical concave relationship between the film thickness and the scanning distance obtained from the P-10 measurements. These concave equations

can be used to predict the profiles formed using various dosing strategies. Figures 7(b)–7(e) clearly depict that the dosing strategy can be used to print concave structures. These SEM micrographs demonstrate the same behavior observed in the P-10 profiles in Figure 6-7(a).

6.3.4 Etching Behaviors of SU-8 Film

In this study, we used RIE to evaluate the etching resistance for SU-8 resists on a silicon dioxide layer. The feeding gas is a mixture of Ar, CHF_3 , and CF_4 . The chemical species existing in the plasma can be expressed as follows:

$$Ar + e^- \rightarrow Ar^+ + 2e^-$$

$$CF_4 + e^- \rightarrow CF_3^+ + F^- + e^-$$

$$CF_3^+ + F^- \rightarrow CF_4$$

$$CF_4 + 2e^- \rightarrow CF_3^- + F^-$$

$$CHF_3 + e^- \rightarrow CF_3^- + H^+ + e^-$$

$$CF_3^+ + CF_3^- \rightarrow C_2F_6$$

$$SiO_2 + CF_3^+ + F^- \rightarrow SiF_4 + CO_2.$$

The generated $CF3^-$ and F^- species in the plasma react with the oxide film to form the volatile species SiF_4 and CO_2 . Through this process, the oxide film becomes etched. In addition, the generated radicals, atoms, and ions can also react with SU-8 resists to form various volatile products such as CO, CO_2, H_2O, OH, and COF_2 . Therefore, the resistance of the resist toward plasma is very important for ensuring etch reliability. Figure 6-8(a) shows that the etching rates of the SU-8 resist and the oxide film decrease upon increasing the relative CHF_3 content. This observation explains the role

of CHF_3 in the plasma. The species generated from CHF_3 in the plasma are H^+ and CF_3^-, and the CF_3^- species can quench the activity of CF_3^+ in the plasma. Hence, the etching rate decreases. Figure 6-8(a) also depicts the etching selectivity. The selectivity gradually increases upon increasing the relative CHF_3 content. The etching behavior of the SU-8 resist on the polysilicon layer was evaluated using an ECR etcher. The feeding gas is a mixture of Cl_2 and O_2. The chemical species existing in the plasma can be expressed as follows:

$$Cl_2 \rightarrow 2Cl$$

$$Si + 2Cl \rightarrow SiCl_2$$

$$SiCl_2 + 2Cl \rightarrow SiCl_4$$

$$O_2 + Cl \rightarrow ClO_2$$

$$ClO_2 + Cl \rightarrow Cl_2 + O_2.$$

The generated Cl species in the plasma react with the polysilicon film, and form the volatile species $SiCl_4$. In addition, the generated radicals, atoms, and ions can also react with the SU-8 resist to form various volatile products, such as HCl and $COCl_2$. The resistance of the resist toward plasma is very important for ensuring the reliability of the etching. Figure 6-8(b) displays that, for SU-8 resists, the etching rate decreases upon increasing the amount of Cl_2. This observation can be explained by considering the relative amount of O_2 in the plasma: a decrease in O_2 ratio decreases its reaction with the carbon-based ingredients of the resist. For the poly-Si film, the increase in the Cl_2 ratio significantly increases the etching rate. The etching rate is very small, however, if the Cl2 ratio is below 0.85. This finding indicates that an O_2 ratio greater

than 0.15 is required to oxidize the poly-Si film quickly. The silicon dioxide that forms is resistant to Cl2 etching. In addition, the etching selectivity displayed in Figure 6-8(b) increases with increasing Cl_2 ratio.

6.3.5 Fabrication of Curved Spiral Structure

The technology for fabricating a nonplanar spiral structure has not been proposed before. In Figure 6-9(a), we propose an electron-beam writing strategy for preparing a nonplanar spiral device. The spiral channel of SU-8 resist is divided into five sections. After exposure with different electronbeam dosages, the height gradually decreases from section I to section V. The figure-of-merit design can save chip area more than any other design. Another great challenge for analyzing the spiral structure is finding a method to characterize the depth profile, since optical and electron microscopes face a problem in the depth of focus. Therefore, as a demonstration in Figure 6-9(a), we require a 2D profiler for 3D mapping in the future. Figure 6-9(b) illustrates the image of the nonplanar spiral channel obtained using an optical microscope. The horizontal and perpendicular profiles are shown in Figure 6-9(c) and 9(d), respectively. These results clearly indicate that the writing strategy developed is very useful for the fabrication of nonplanar spiral structures.

3.4 CONCLUSIONS

SU-8 film was exposed to a shaped electron beam, and we evaluated its sensitivity, chemical reactivity, and thermal stability toward treatment with an oxygen plasma, as well as its etching performance. The oxygen plasma was used to stabilize the chemical bond and the film through polymerization. An electron-beam writing strategy is presented in this study and it was employed successfully to fabricate

curved devices, such as convex, concave, and spiral structures.

REFERENCES

1. P. Wilding; L. J. Kricka; J. Cheng; G. Hvichia; M. A. Shoffner; P. Fortina; *Anal. Biochem*. **257**, 95 (1998).

2. T. Deng; F. Arias; R. F. Ismagilov; P. J. A. Kenis; G. M. Whitesides; *Anal. Chem.* **72**, 645 (2000).

3. A. J. Gawron; R. S. Martin; S. M. Lunte. *Eur. J. Pharm. Sci.* **14**, 1 (2001).

4. Y. M. Huang; C. P. Jiang. *Int. J. Adv. Manuf. Tech.* **21**, 649 (2003).

5. L. A. Tse; P. J. Hesketh; D. W. Rosen. *Microsyst. Technol*. **9**, 319 (2003).

6. K. J. Boyd; A. Lapicki; M. Aizawa; S. L. Anderson. *Rev. Sci. Instrum.* **69**, 4106 (1998).

7. S. Reyntjens; R. Puers. *J. Micromech. Microeng.* **10**, 181 (2000).

8. R. G. Woodham; H. Ahmed. *J. Vac. Sci. Technol. B* **17**, 3075 (1999).

9. S. T. Davies; B. Khamsehpour. *Vacuum* **47**, 455 (1996).

10. N. Gottschlich; S. C. Jacobson; C. T. Culbertson; J. M. Ramsey. *Anal. Chem*. **73**, 2669 (2001).

11. H. L. Chen; C. H. Chen; F. H. Ko; T. C. Chu; C. T. Pan; H. C. Lin. *J. Vac. Sci. Technol. B* **20**, 2973 (2002).

12. *International Technology Roadmap for Semiconductors*, SIA Publication (Semiconductor Industry Association, 2001).

13. V. Kudryashov; X. C. Yuan; W. C. Cheong; K. Radhakrishnan; *Microelectron. Eng.* **67–68**, 306 (2003).

14. J. Yao; Z. Cui; F. Gao; Y. Zhang; Y. Guo; C. Du; H. Zeng; C. Qiu. *Microelectron. Eng.* **57–58**, 729 (2001).

15. W. Daschner; P. Long; S. Stein; C.Wu; S. H. Lee. *Appl. Opt*. **36**, 4675 (1997).

16. V. A. Kudryashov; P. D. Prewett; A. G. Michette. *Microelectron. Eng.* **46**, 209 (1999).

17. H. Becker; L. E. Locascio. *Talanta* **56**, 267 (2002).

18. J. R. Sheats; B. W. Smith. *Microlithography Science and Technology* (Marcel Dekker, New York, 1998).

19. L. F. Thompson; C. G. Wilson; M. J. Bowden. *Introduction to Microlithography* (ACS Publications, Washington, D.C., 1994).

20. W. G. Kim; J. Y. Lee. *Polymer*, **43**, 5713 (2002).

21. K. Mimura; H. Ito, *Polymer*, **43**, 7559 (2002).

Table 6-1. Operating conditions for the reactive ion etcher.

	Step 1	Step 2
Pressure/Torr	0.2	0.2
RF power/W	0	500
Gas flow rate/cm^3min^{-1}		
Ar	400	400
CHF_3	10-30	10-30
CF_4	30-10	30-10

Table 6-2. Operating conditions for the electron cyclotron resonance etcher.

	Step 1	Step 2
Pressure/Torr	3 ×10^{-3}	3 ×10^{-3}
Power/W		500
Source, Microwave power	0	250
Back side, RF Power	0	90
Gas flow rate/cm^3min^{-1}		
Cl_2	50	40-50
O_2	0	0-10

Table 6-3. The fitting equations obtained from the relationship between the SU-8 film thickness and the scanning distance for the preparation of non-planar structures.

unit distance	convex profile	concave profile
3 μm	$y=0.0074x^4-0.0283x^3+0.2958x^2+0.2672x+0.613$	$y=0.0494x^2+0.177x$
5 μm	$y=0.0002x^4-0.0104x^3+0.1476x^2+0.3484x-0.042$	$y=0.0227x^2+0.1762x$
7 μm	$y=6\times10^{-5}x^4-0.0041x^3+0.073x^2+0.4333x-0.1566$	$y=0.0175x^2+0.1237x$
9 μm	$y=2\times10^{-5}x^4-0.016x^3+0.031x^2+0.5164x-0.301$	$y=0.0053x^2+0.0807x$
15 μm	$y=1\times10^{-5}x^4-0.001x^3+0.0012x^2+0.5433x-0.3228$	$y=0.0009x^2+0.1058x$
20 μm	$y=3\times10^{-7}x^4-5\times10^{-5}x^3+0.004x^2+0.3863x-0.1233$	$y=0.0007x^2+0.0725x$
25 μm	$y=2\times10^{-7}x^4-5\times10^{-5}x^3+0.002x^2+0.2409x-0.031$	$y=0.0005x^2+0.0393x$

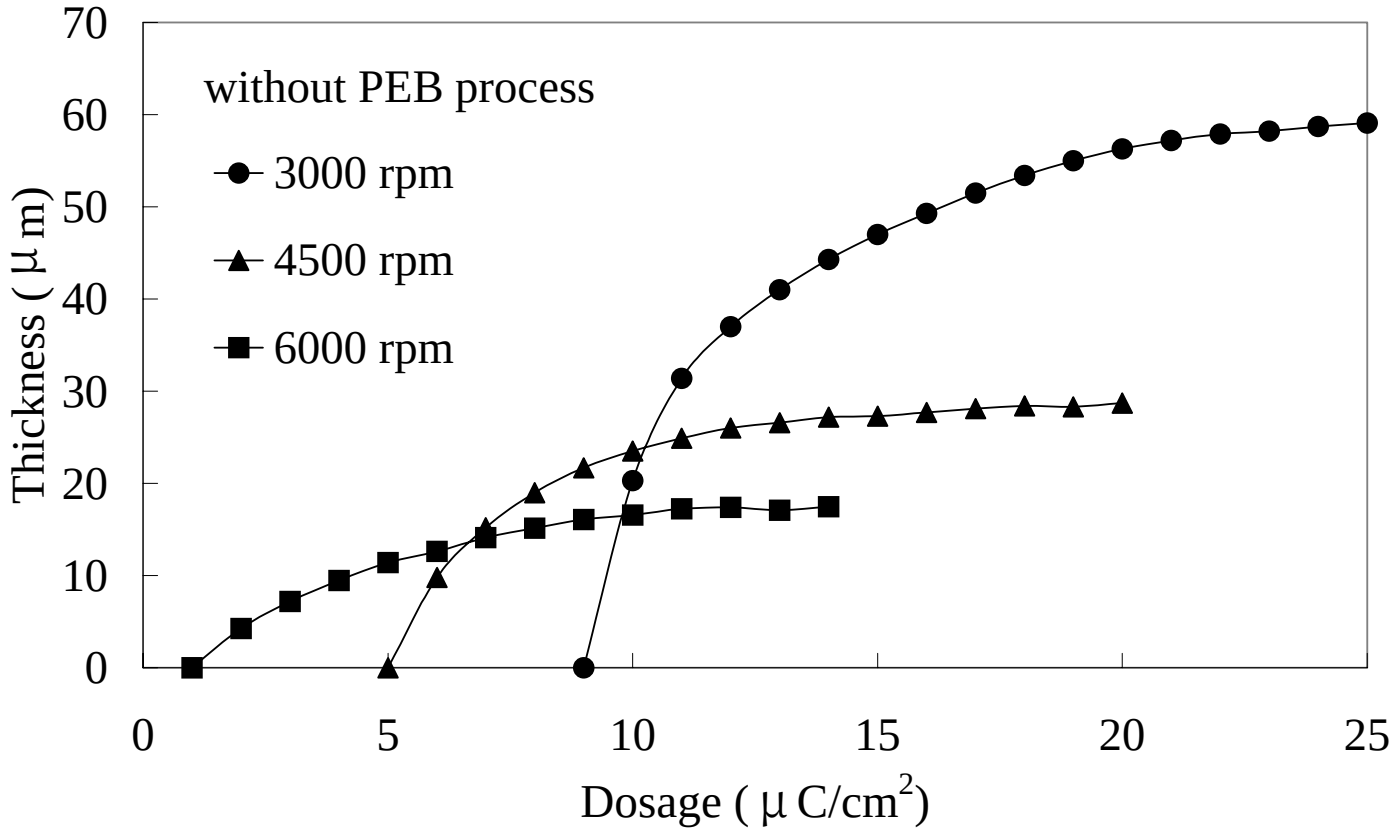

Figure 6-1. Sensitivity curves for three thicknesses of the SU-8 resist at an electron-beam exposure of 40 keV

(a)

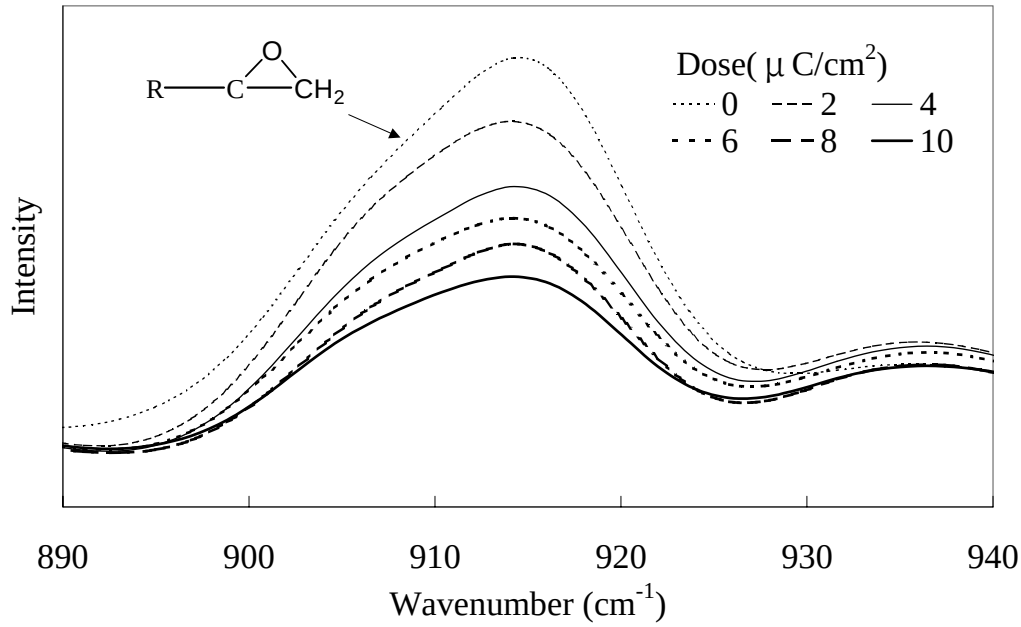

(b)

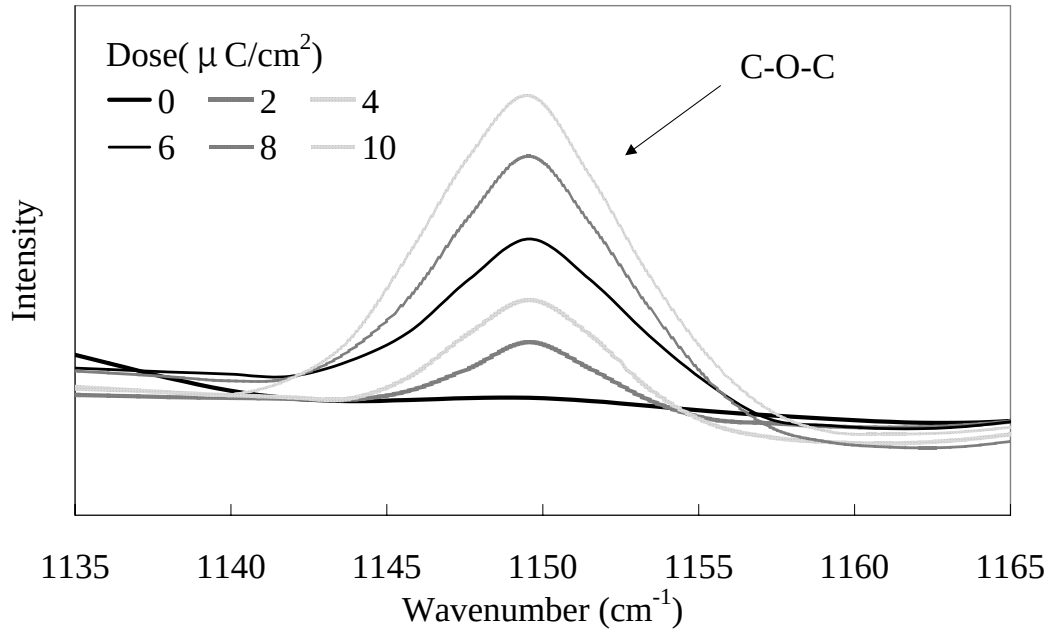

Figure 6-2. FTIR spectra of SU-8 films having been subjected to various doses of an electron beam. (a) The characteristic absorption near 915 cm^{-1} after exposure at 0, 2, 4, 6, 8, and 10 $\mu C/cm^2$. (b) The characteristic absorption near 1150 cm^{-1} after exposure at 0, 2, 4, 6, 8, and 10 $\mu C/cm^2$.

(c)

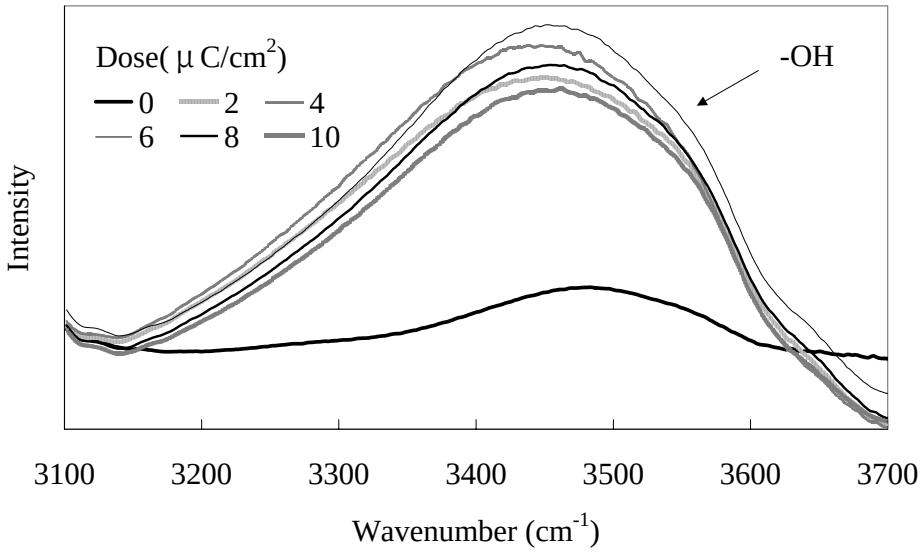

(d)

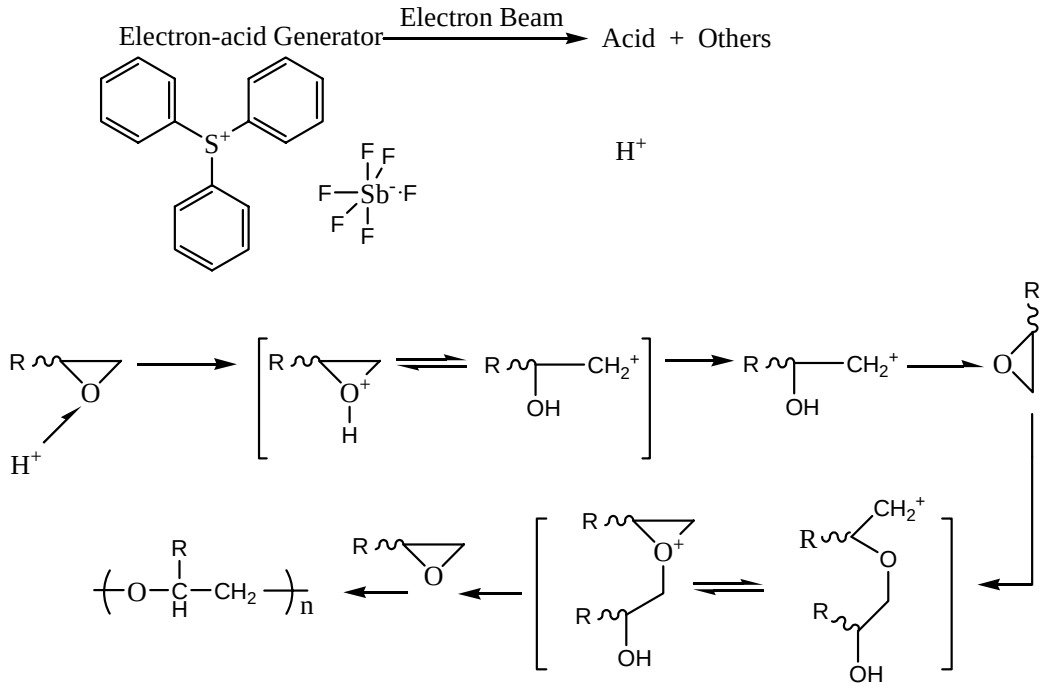

Figure 6-2. (c)FTIR spectra of SU-8 films having been subjected to various doses of an electron beam with the characteristic absorption near 3450 cm^{-1} after exposure at 0, 2, 4, 6, 8, and 10 $\mu C/cm^2$. (d) The reaction mechanism of SU-8 films after shaped electron beam exposure.

(a)

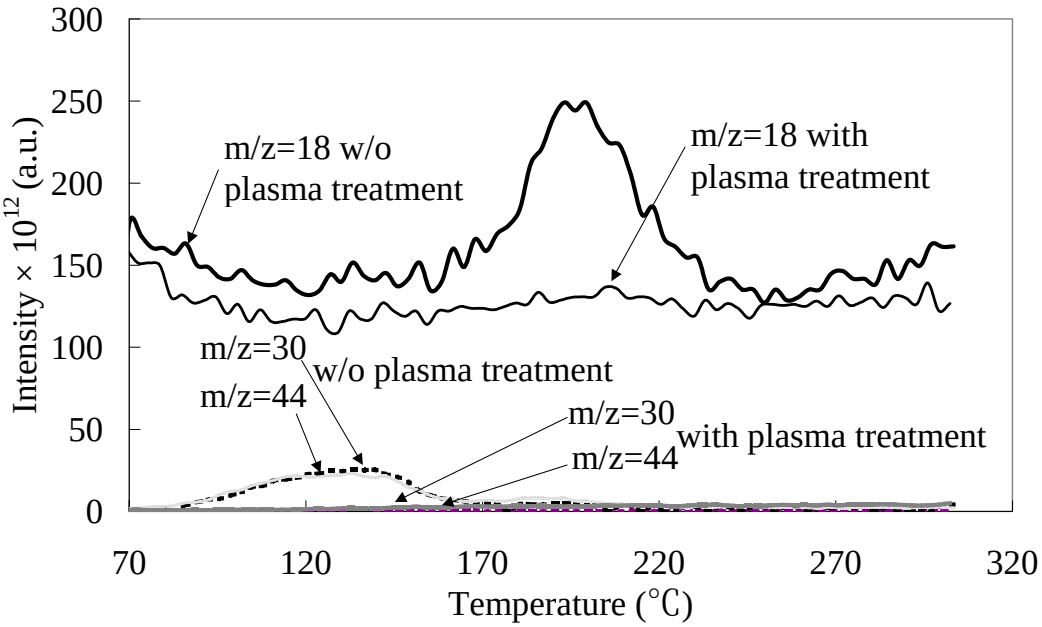

(b) (c)

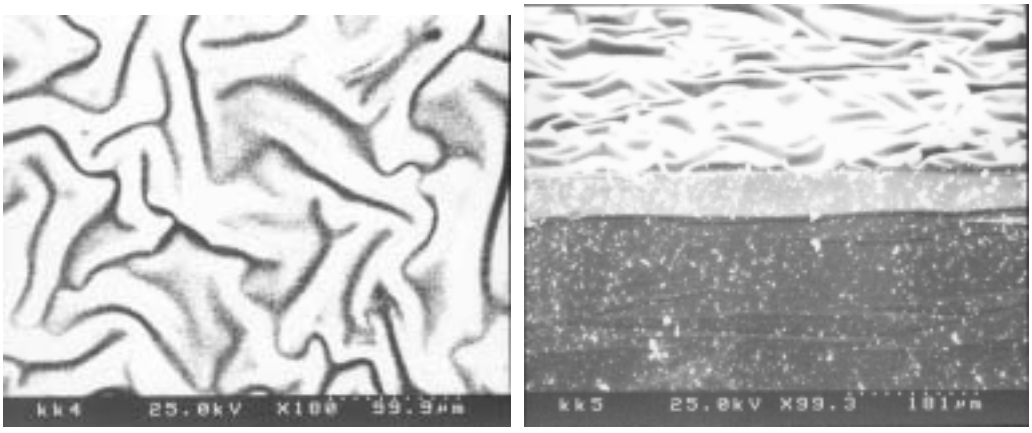

Figure 6-3. (a) The out-gassing mass spectra at various desorption temperatures with and without oxygen plasma treatment. (b) Top-down SEM images of SU-8 film treated with oxygen plasma for 60 s. (c) Cross-sectional view of (b).

(a)

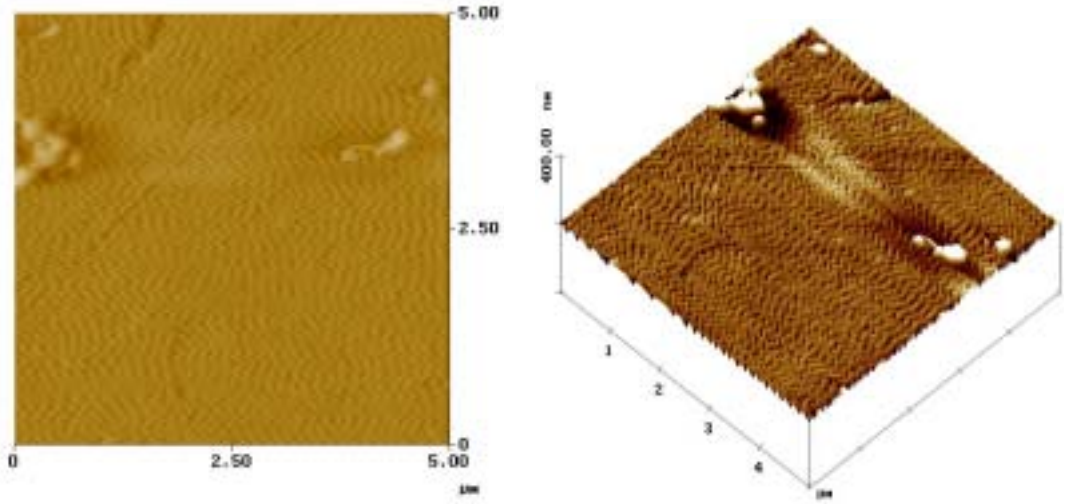

(b)

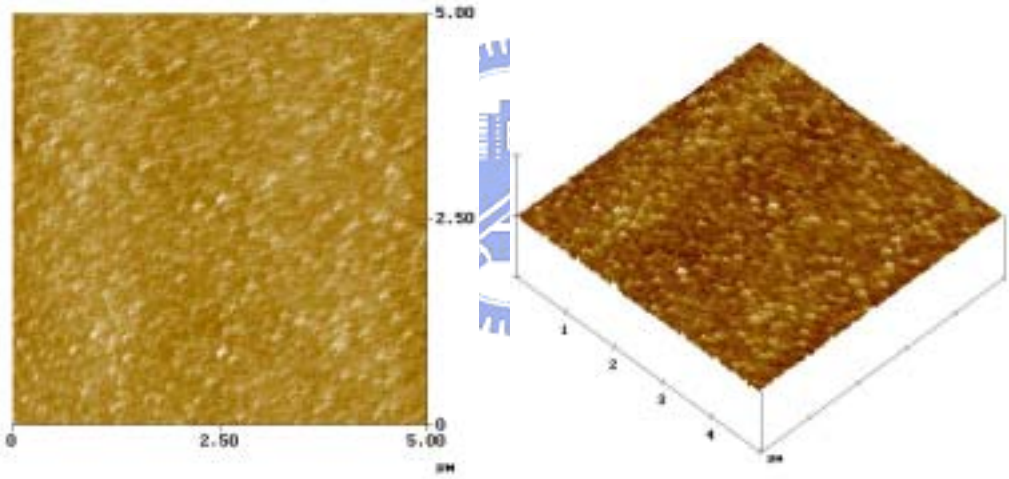

Figure 6-4. AFM images of the SU-8 film treated after treatment with oxygen plasma for (a) 0, and (b) 20 s.

(c)

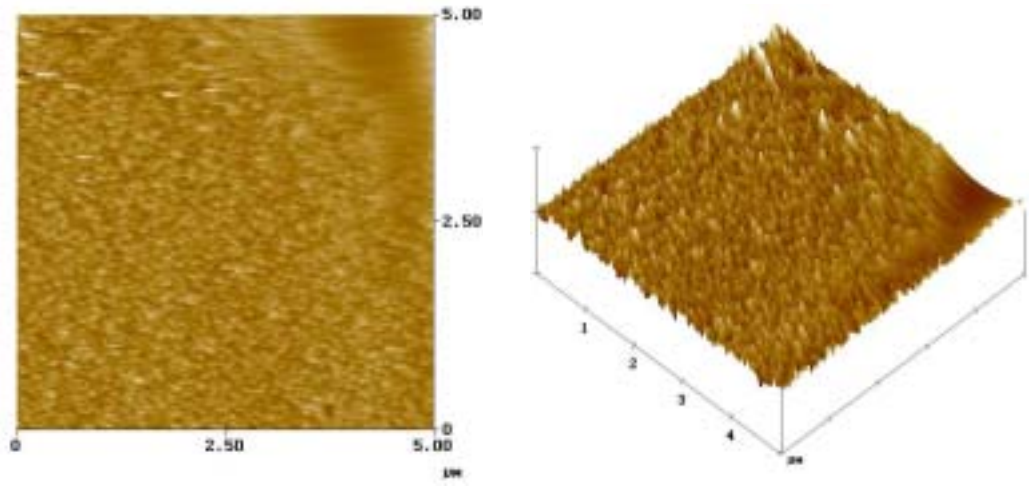

(d)

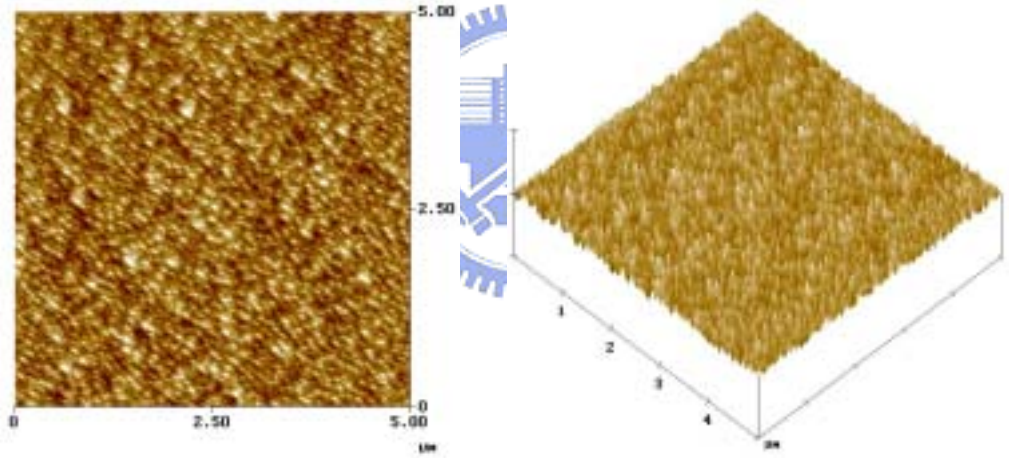

Figure 6-4. AFM images of the SU-8 film treated after treatment with oxygen plasma for (c) 40, and (d) 60 s.

(a)

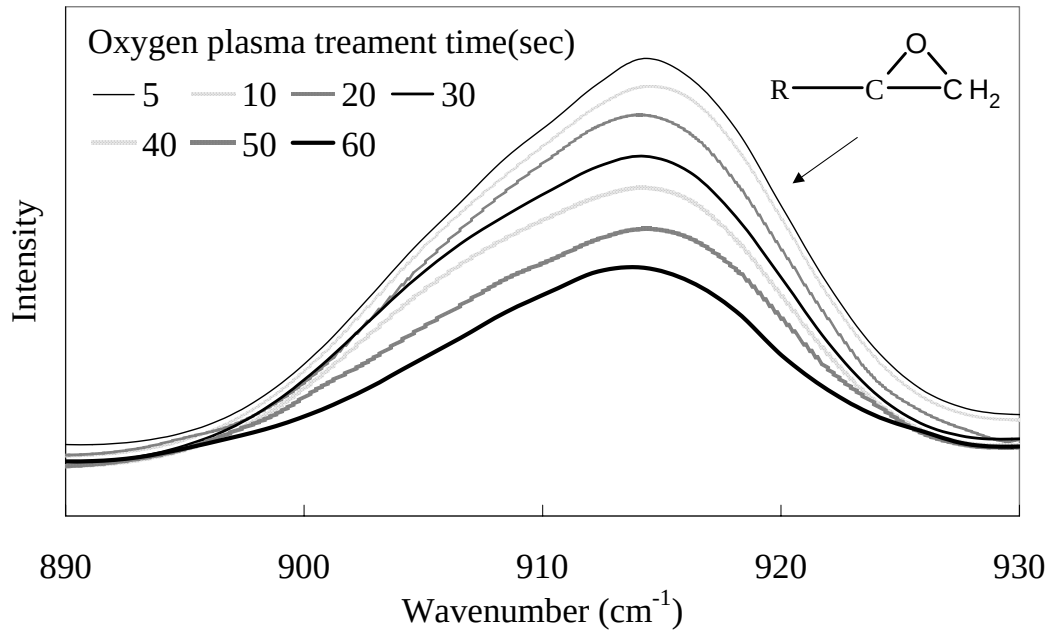

(b)

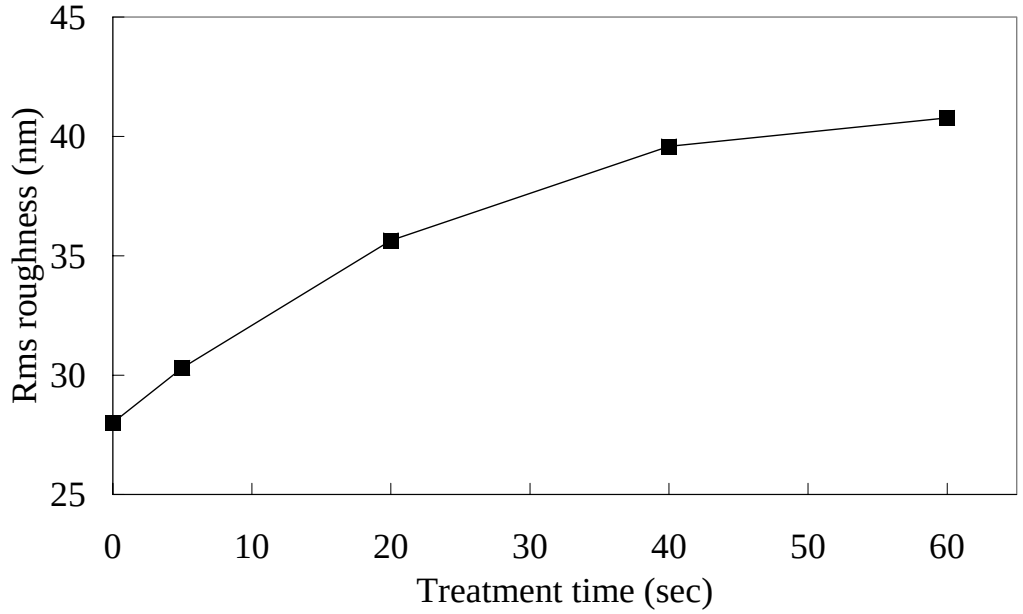

Figure 6-5. (a) FTIR spectra of SU-8 films having been subjected to various reaction times with oxygen plasma. (b) Effect of the oxygen plasma treatment time on the surface roughness of SU-8 film.

(a)

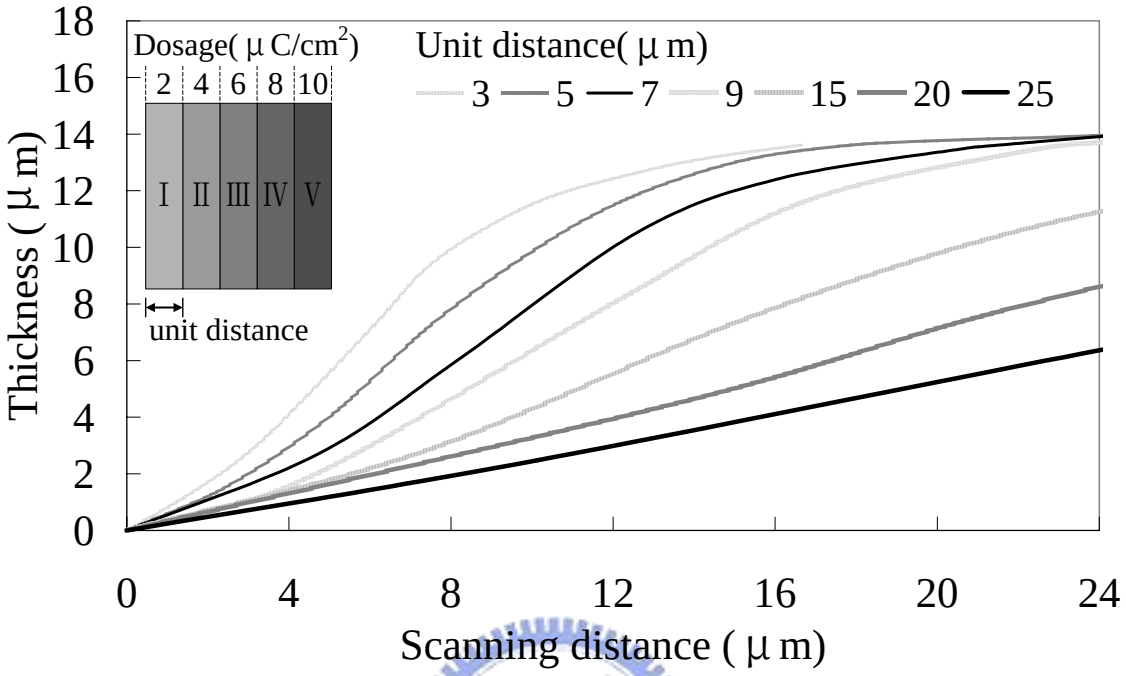

Figure 6-6. Three-dimensional profiles of the SU-8 film that were designed using electron-beam writing technology. (a) Convex profile formed by various doses on the unit distance with the convex profile at unit distances of 3, 5, 7, and 10 μm.

(b) (c)

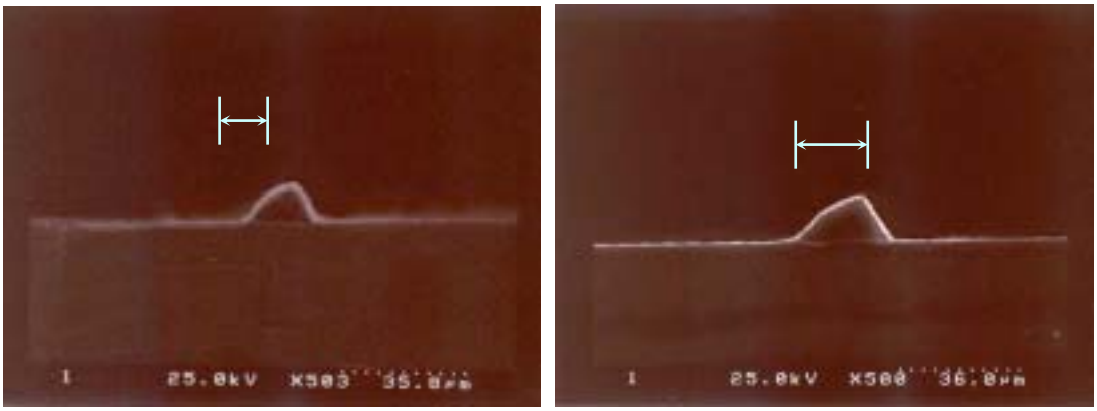

(d) (e)

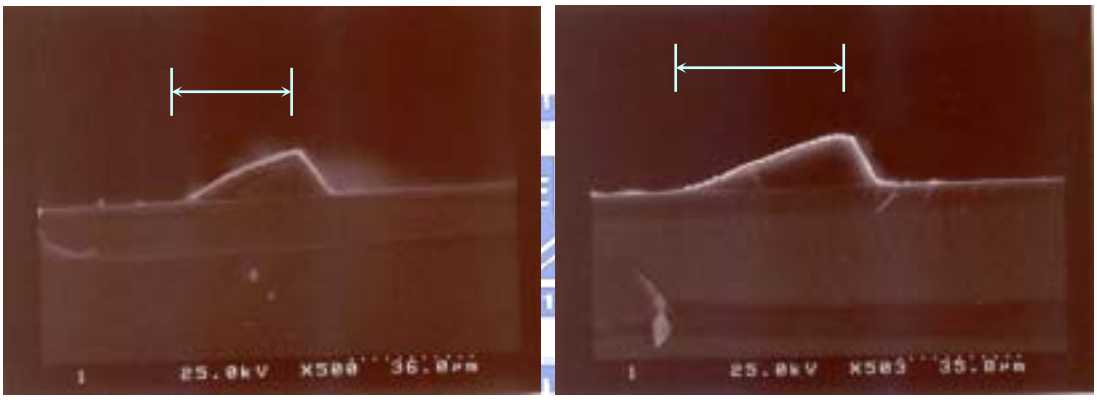

Figure 6-6. Three-dimensional profiles of the SU-8 film that were designed using electron-beam writing technology. The cross-sectional SEM images of the convex profile at unit distances of (b) 3, (c) 5, (d) 7, and (e) 10 μm.

(a)

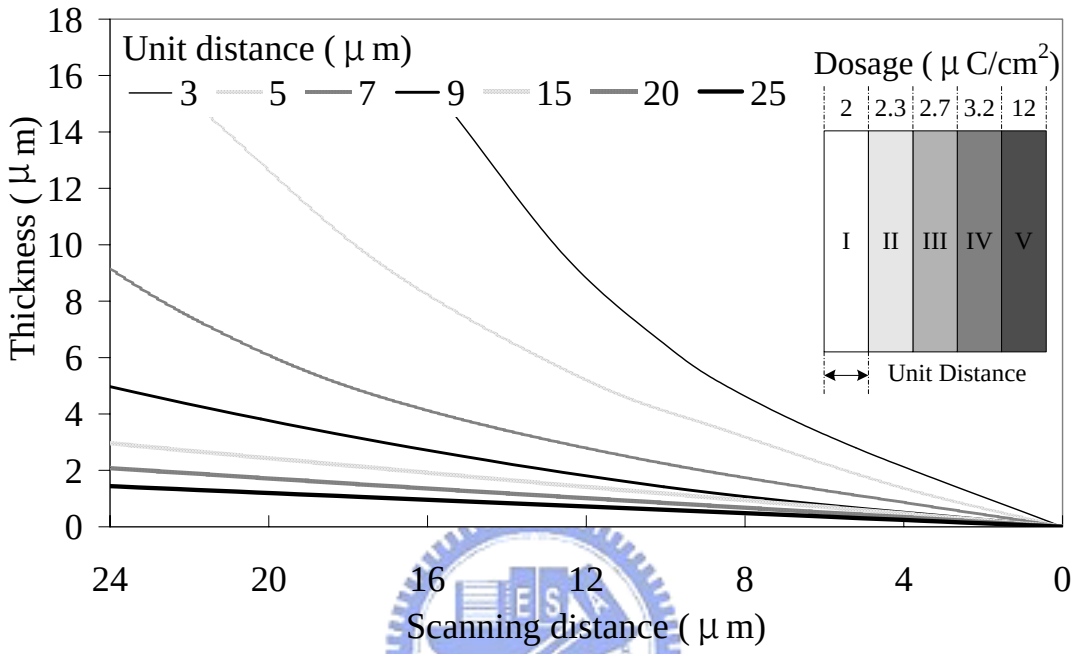

Figure 6-7. Three-dimensional profiles of the SU-8 film that were designed using electron-beam writing technology. (a) Concave profile formed by various doses on the unit distance with the concave profile at unit distances of 3, 5, 7, and 10 μm.

(b) (c)

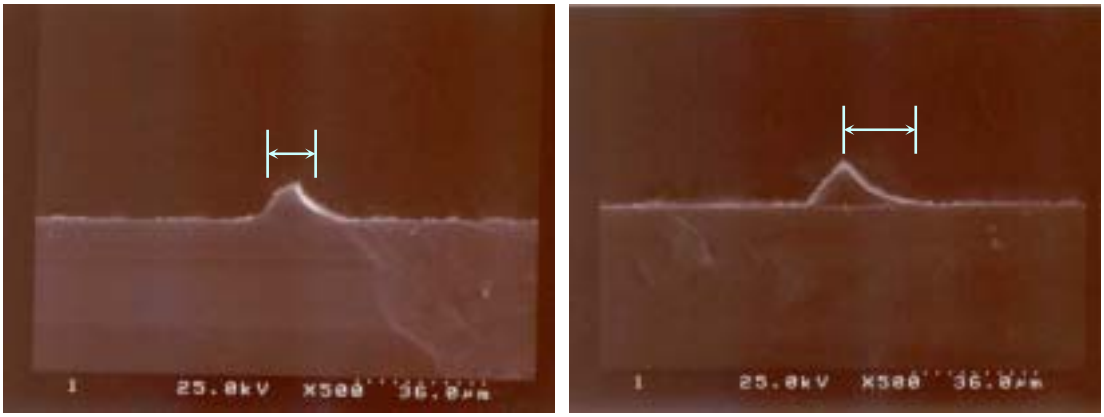

(d) (e)

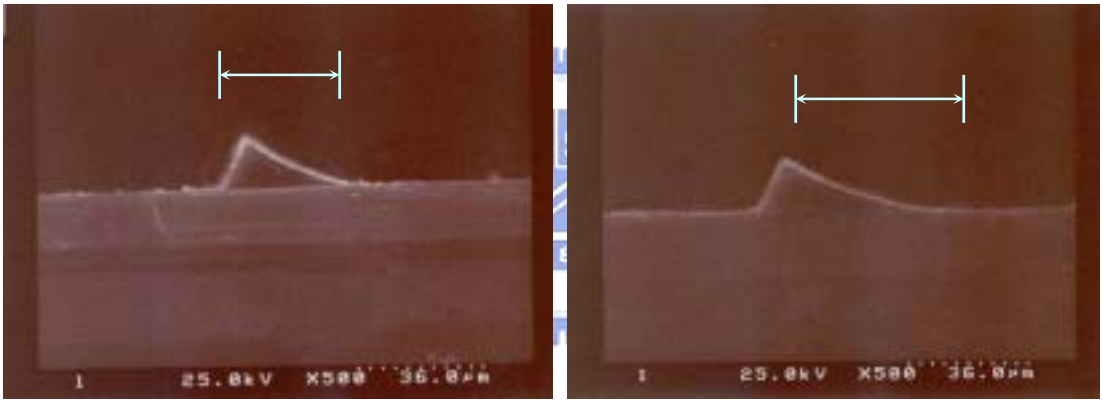

Figure 6-7. Three-dimensional profiles of the SU-8 film that were designed using electron-beam writing technology. (a) The cross-sectional SEM images of the concave profile at unit distances of (b) 3, (c) 5, (d) 7, and (e) 10 μm.

(a)

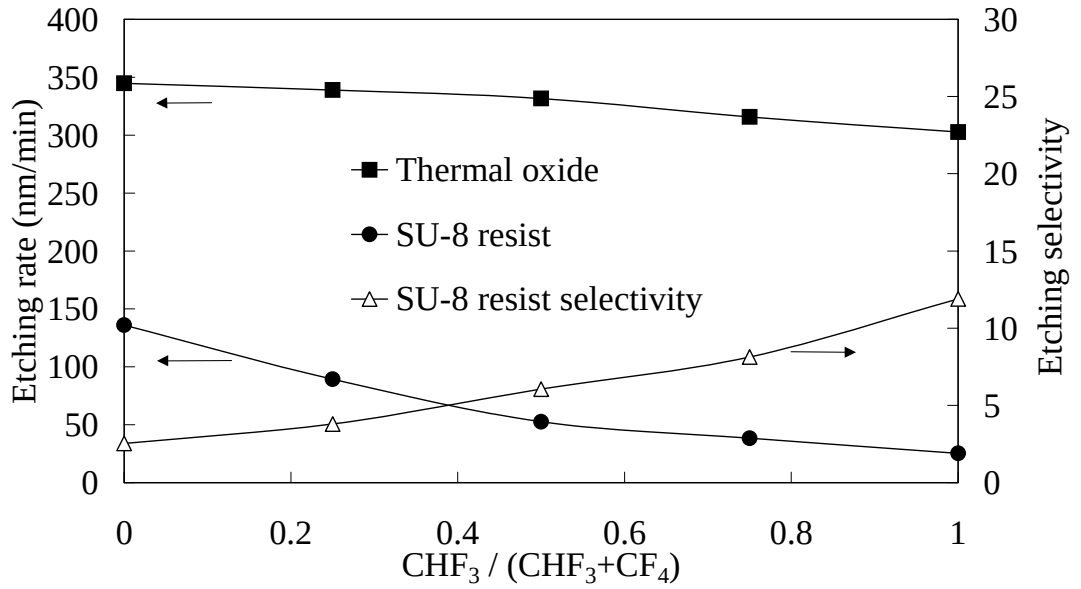

(b)

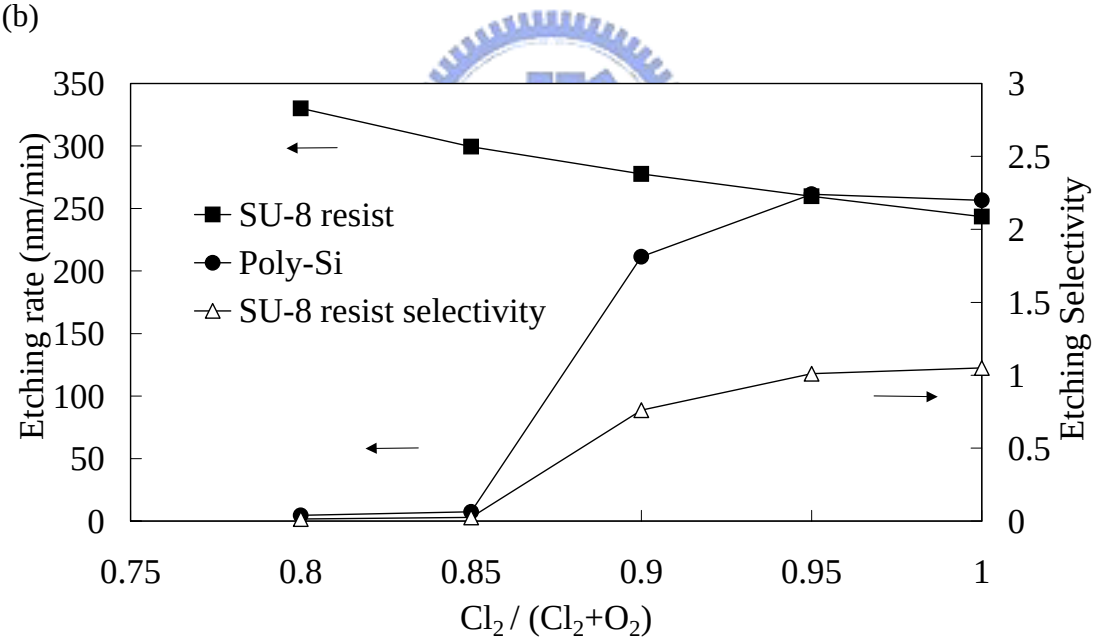

Figure 6-8. The etching rate and selectivity of (a) the $CHF_3/(CHF_3 + CF_4)$ gas ratio for thermal oxide and SU-8 films, and (b) the $Cl_2/(Cl_2 + O_2)$ gas ratio for poly-Si and SU-8 films.

(a)

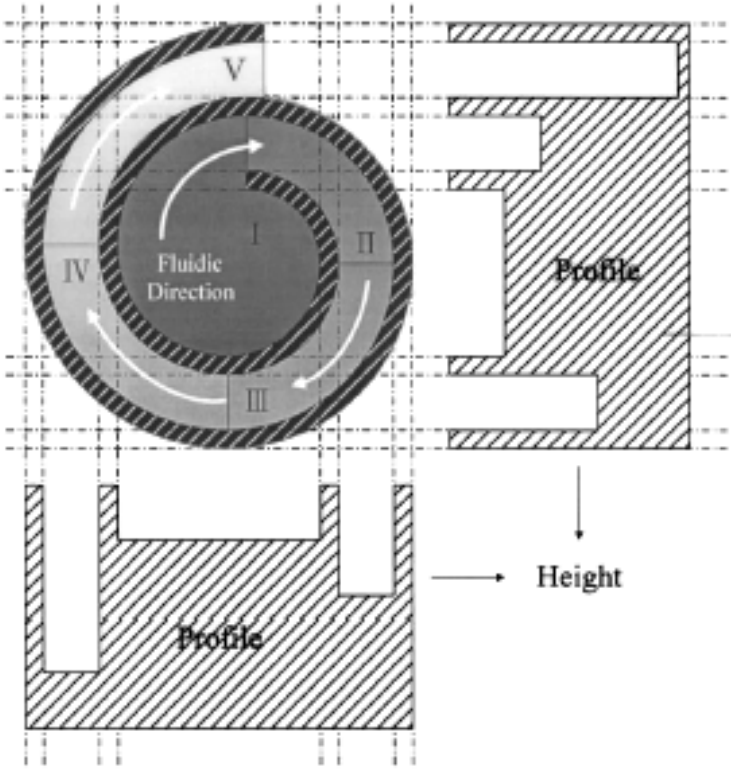

(b)

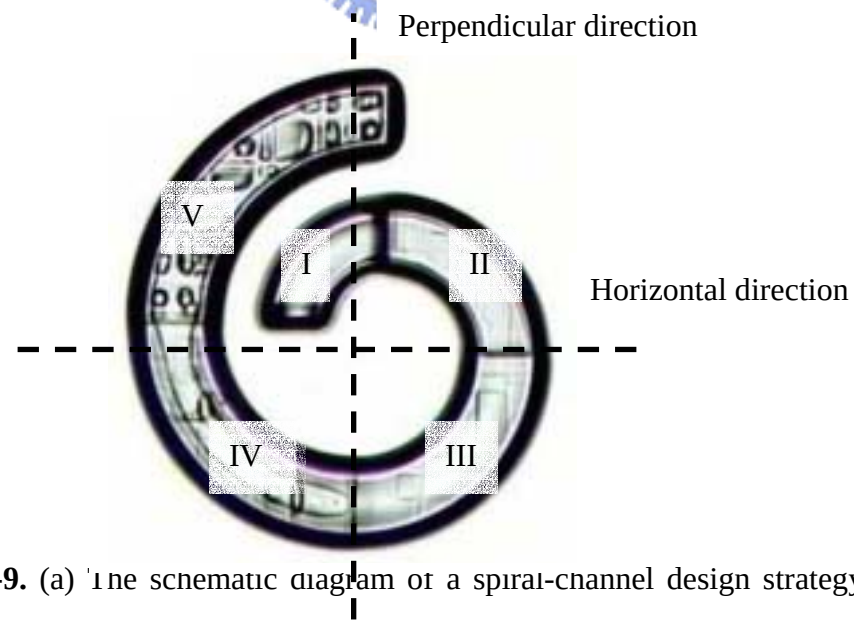

Figure 6-9. (a) The schematic diagram of a spiral-channel design strategy. (b) The optical microscope image of the fabricated spiral channel.

(c)

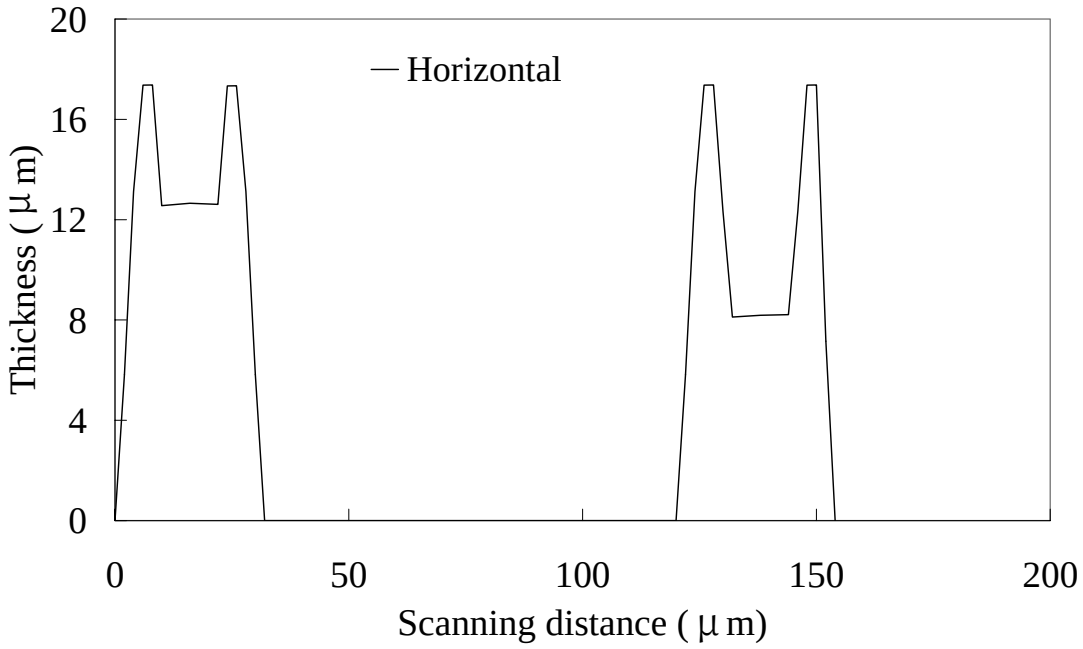

(d)

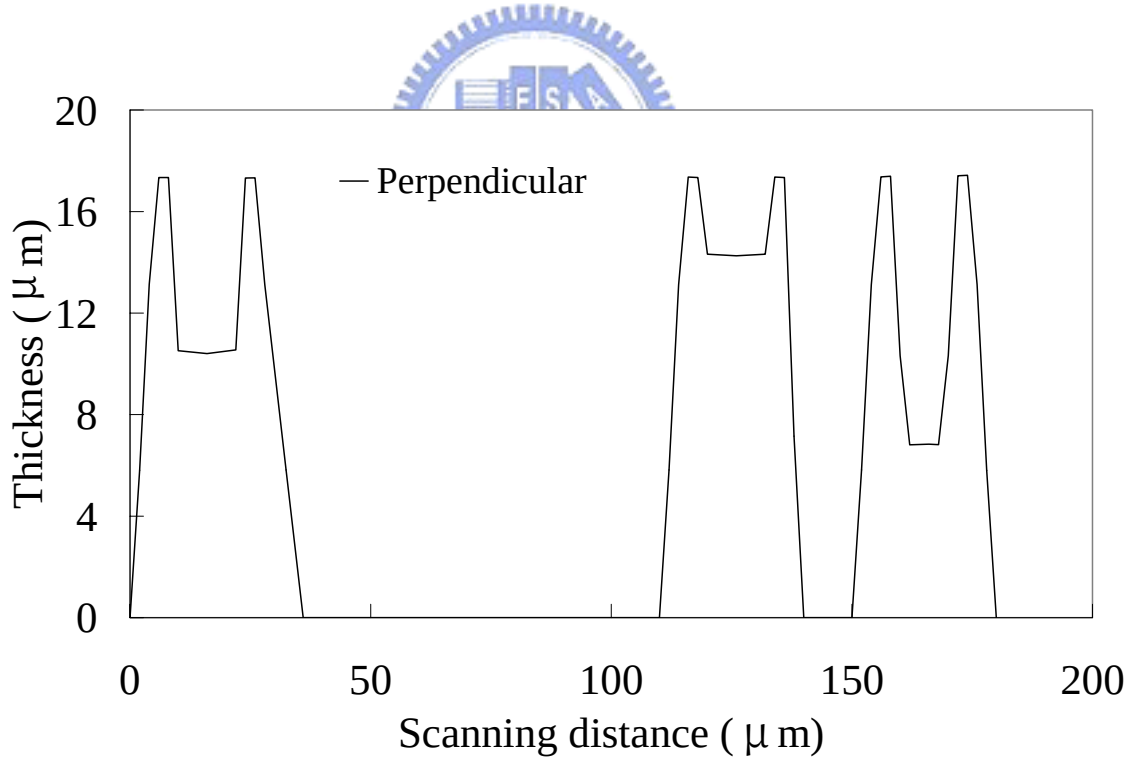

Figure 6-9. (c) The horizontal profile of the spiral channel obtained by a surface profiler measurement. (d) The perpendicular profile of the spiral channel obtained by a surface profiler measurement.